# Multichannel recombination in high-order-harmonic generation from asymmetric molecular ions

Xiang-Yang Miao* and Cai-Ping Zhang
*College of Physics and Information Engineering, Shanxi Normal University, Linfen 041004, China*
(Received 12 October 2013; published 10 March 2014)

The multichannel recombination in high-order-harmonic generation (HHG) from the asymmetric molecular ion $HeH^{2+}$ has been investigated by numerically solving the time-dependent Schrödinger equation based on the non-Born-Oppenheimer approximation. In this paper, not only has the physical image in harmonic emission from the asymmetric molecular ion been established, but also the distinguishing of recombination channels has been achieved. Moreover, our quantitative calculations show that the recombination channels from different electronic states make different contributions to HHG. Furthermore, by means of the time-frequency maps, electron-nuclear probability density distributions, and the laser dressed state picture, the physical mechanism of the multichannel recombination has been revealed.

DOI: 10.1103/PhysRevA.89.033410 PACS number(s): 33.80.Rv, 34.50.Gb, 42.50.Hz

## I. INTRODUCTION

High-order-harmonic generation (HHG) from atoms [1,2] and molecules [3] in the intense laser field has been viewed as an important tool for obtaining a coherent attosecond laser pulse [4], which is important for imaging the structure of the molecule [5] and investigating the ultrafast electronic dynamics [1,6,7]. The related physical process can be well explained through the semiclassical three-step model [8–10]: The electron is first ionized through tunneling from the ground state, then is accelerated in the external laser field, and finally recombines into the ground state followed by harmonic emission. Obviously, both the ionization and recombination processes occur in the ground state [11].

However, recent studies have shown that not only the ground state but the excited state contributes to the HHG spectrum [11]. For the symmetric molecules, such as $H_2^+$ [12,13], the message of the excited state is mainly recorded in the interference minimum of the HHG spectrum. Bao *et al.* [14] employed the $H_2^+$ prepared in a coherent superposition of the two lowest-lying states to examine the interference between different recombination paths in harmonic yields. Han and Madsen [15] made further investigation about the role of excited states in HHG from $H_2^+$. With the increase of the internuclear distance, the recombination into the first excited state tends to dominate and the interference minimum in the spectrum is ascribed to the orbital interference. For asymmetric molecules, with longer mean lifetime of the first excited state [16–18], some novel effects have been discovered. For example, Bian and Bandrauk [19–22] proposed the four-step model of molecular high-order-harmonic generation (HHG) from $HeH^{2+}$, and the excited state shows itself obviously in lower harmonics where the resonance between the ground and excited states takes place. Moreover, Feng and Chu [11] adopted $LiH^{3+}$ and $BeH^{4+}$ besides the $HeH^{2+}$ to prove that this excited state effect is a general character of the asymmetric molecules. Chen and Zhang [23] discovered that for each optical cycle, the emission times of the harmonics follow two characteristic electron trajectories based on the ground and excited states, respectively. And it can be used as an efficient tool to probe the dynamics of the excited state of the asymmetry molecule. Lu *et al.* [24] found that when the initial wave packet of $HeH^{2+}$ is prepared in the first excited state, the high-intensity single attosecond pulse could be obtained by selecting appropriate carrier-envelope phase.

Recently, the relevant studies about HHG from asymmetric molecules are mainly based on the Born-Oppenheimer (BO) approximation ignoring the couplings of the electronic and nuclear wave packet [11,19–23]. However, Liu *et al.* [25] have revealed that the nuclear motion greatly affects the molecular HHG from $H_2^+$. Kreibich *et al.* [26] have also reported the non-BO effect in harmonic generation. With the interaction of the strong laser pulse, the nuclear probability density will expand to a larger internuclear distance and it may influence the asymmetric molecular HHG. In this paper, by considering the coupling of electronic and nuclear wave packets, we have deeply investigated the multichannel recombination in harmonic emission from $HeH^{2+}$. Not only have the recombination channels resulting from the contribution of the ground $1s\sigma$ and first excited $2p\sigma$ states been distinguished, but also the contributions of these channels to the harmonic emission have been analyzed quantitatively. The results show that the $H \rightarrow e \rightarrow H$ ($He \rightarrow e \rightarrow H$) channel is prominent for the $2p\sigma$-state-based ionization ($1s\sigma$-state-based ionization).

The paper is arranged as follows: The numerical method is presented in Sec. II; detailed numerical results and discussion are provided in Sec. III; our concluding remarks follow in Sec. IV.

## II. NUMERICAL METHOD

The one-dimensional (1D) calculation for an asymmetric diatomic molecule ($HeH^{2+}$) in the intense laser field has been performed by numerically solving the time-dependent Schrödinger equation (TDSE) based on the non-BO approximation including both the electronic and nuclear motions. The first excited $2p\sigma$ state of the $HeH^{2+}$ is a bound state with a long lifetime of about 4 ns [19–22], which may induce the transition of the wave packets between the ground $1s\sigma$ state and the excited $2p\sigma$ state in strong laser field, so $HeH^{2+}$ is prepared in the $2p\sigma$ state in our numerical simulation. Providing the linear laser field along with the internuclear axis and ignoring the rotation of the molecular axis, in the dipole approximation

*sxxymiao@126.com

 

and the length gauge, the TDSE reads as

$$i\frac{\partial\psi(R,z;t)}{\partial t} = [H_0 + V(t)]\,\psi(R,z;t), \tag{1}$$

where $H_0 = T_n + T_e + V_c$ is the field-free Hamiltonian with

$$T_n = -\frac{1}{2\mu_n}\frac{\partial^2}{\partial R^2}, \tag{2}$$

$$T_e = -\frac{1}{2\mu_e}\frac{\partial^2}{\partial z^2}, \tag{3}$$

$$V_c = \frac{C_{\rm He}C_{\rm H}}{\sqrt{R^2+a}} - \frac{C_{\rm H}}{\sqrt{(z-z_{\rm H})^2+b}} - \frac{C_{\rm He}}{\sqrt{(z-z_{\rm He})^2+b}}, \tag{4}$$

where $R$ is the internuclear distance and $z$ is the electron coordinate (with respect to the nuclear center of mass). $C_{\rm He}$ and $C_{\rm H}$ are the electric charges of the nuclei. $z_{\rm H} = \frac{M_{\rm He}R}{M_{\rm H}+M_{\rm He}}$ and $z_{\rm He} = -\frac{M_{\rm H}R}{M_{\rm H}+M_{\rm He}}$ present the positions of the nucleus $H^+$ and the nucleus $He^{2+}$, respectively. $\mu_n = (\frac{1}{M_{\rm H}} + \frac{1}{M_{\rm He}})^{-1}$ and $\mu_e = \frac{M_{\rm H}+M_{\rm He}}{M_{\rm H}+M_{\rm He}+1}$ are the reduced masses with $M_{\rm H}$ and $M_{\rm He}$ the masses of H and He. The soft-core parameters $a = 0.01$ and $b = 0.3$ have been adopted to match the ionization potential of $2p\sigma$ bound state and equilibrium distance of 1.03 and 3.89 a.u. [16], respectively.

In the dipole approximation and the length gauge, $V(t)$ is the electric potential including the interaction between $HeH^{2+}$ and the intense laser field, and the corresponding form is [27,28]

$$V(t) = \left[\frac{C_{\rm He}M_{\rm H} - C_{\rm H}M_{\rm He}}{M_{\rm H}+M_{\rm He}}R + \left(1 + \frac{C_{\rm H}+C_{\rm He}-1}{M_{\rm He}+M_{\rm H}+1}\right)z\right] E(t), \tag{5}$$

$$E(t) = E_0 f(t)\cos(\omega t), \tag{6}$$

where $E_0$ and $\omega$ are the peak intensity and laser frequency, respectively. $f(t)$ is the pulse envelope of time duration 7 optical cycles (o.c.) trapezoidal shape with 2 cycles ramp on, 3 cycles constant, and 2 cycles ramp off. Additionally, 1 o.c. = 4.005 fs corresponds to the wavelength (1200 nm) of the laser field.

The time-dependent wave function is advanced using the standard second-order split-operator method [29–35],

$$\psi(R,z;t+\delta t) = e^{-iT\,\delta t/2}e^{-iV\delta t}e^{-iT\,\delta t/2}\psi(R,z;t) + O(\delta t^3), \tag{7}$$

where $T$ is the kinetic energy operator and $V$ is the interaction potential taking all the potential energy of the system plus a purely imaginary term to produce an absorbing boundary. In the numerical simulation, the converged numerical parameters are as follows: The grid ranges from 0 to 30 a.u. in the $R$ direction and from $-100$ to 100 a.u. in the $z$ direction, with 299 and 999 points, respectively. With the exponential decay mask function employed in the work, the corresponding absorbing positions are 50 and 100 grid points away from the boundaries in the $R$ direction and $z$ direction, respectively. The corresponding time step is set to be $\delta t = 0.1$ a.u.

The HHG spectrum $[P_A(w)]$ can be obtained by Fourier transforming the time-dependent dipole acceleration $a(t)$,

$$P_A(\omega) = \left|\frac{1}{\sqrt{2\pi}}\int a(t)e^{-i\omega t}dt\right|^2, \tag{8}$$

where $a(t)$ is given by means of Ehrenfest's theorem [36],

$$a(t) = \langle\psi(R,z;t)|\left(-\frac{\partial V_c}{\partial z} + \left(1 + \frac{C_{\rm H}+C_{\rm He}-1}{M_{\rm He}+M_{\rm H}+1}\right)\right) \times E(t)\,|\psi(R,z;t)\rangle\,. \tag{9}$$

To make detailed information of the multichannel recombination in harmonic emission from the asymmetric molecular ion, the time-frequency distribution by means of the windowed Fourier transform has been shown [37],

$$d_\omega(t) = \int a(t')\sqrt{\omega_0}W(\omega_0(t'-t))dt', \tag{10}$$

where $W(\omega_0(t'-t))$ is the mother wavelet expressed as [38]

$$W(x) = \left(\frac{1}{\sqrt{\alpha}}\right)e^{ix}e^{-x^2/2\tau^2}. \tag{11}$$

## III. NUMERICAL RESULTS AND DISCUSSION

### A. Distinguishing of recombination channels in harmonic emission

When the $HeH^{2+}$ is irradiated by the intense laser pulse, the long lifetime of the $2p\sigma$ state makes the wave packets transfer between the $2p\sigma$ and $1s\sigma$ states. In addition, the electronic probability density of the $1s\sigma$ state is mainly localized on the nucleus $He^{2+}$, while the electronic probability density of the $2p\sigma$ state is on the nucleus $H^+$. As a result, the transition between the $2p\sigma$ and $1s\sigma$ states corresponds to the electron transfer from the nucleus $H^+$ to the nucleus $He^{2+}$ [19,20,22]. During the interaction with the strong laser pulse, the electrons may be ionized either from the nucleus $H^+$ or from the nucleus $He^{2+}$, and then multichannel recombination will contribute to the harmonic emission.

In Fig. 1 we schematically plot the physical model for the multichannel recombination in harmonic emission from the $HeH^{2+}$. The black dashed and black solid lines represent the energy combined with the Coulomb and static field potential for $F > 0$ and $F < 0$, respectively. The amplitude $|F|$ corresponds to the peak laser intensity. The green (magenta) circles represent the electrons on the $2p\sigma$ state ($1s\sigma$ state), and red (black or blue) circles represent the ionized (recombined or transferred) electrons. The red (black or blue) lines illustrate the ionization (recombination or transfer) process. Figure 1(a) illustrates the recombination channels originating from the ionized electrons on the $2p\sigma$ state (i.e., around the nucleus $H^+$). On the one hand, some electrons around the nucleus $H^+$ are ionized at the peak intensity, and then are accelerated in the laser field; finally, when the laser field reverses the direction, the electrons may return and recombine with the neighboring ion $He^{2+}$ (channel 1: $H \to e \to He$) or the parent ion $H^+$ (channel 2: $H \to e \to H$). On the other hand, others may be directly transferred from the nucleus $H^+$ to the nucleus $He^{2+}$. When the laser field changes its direction, those electrons may go back and recombine with the nucleus $H^+$

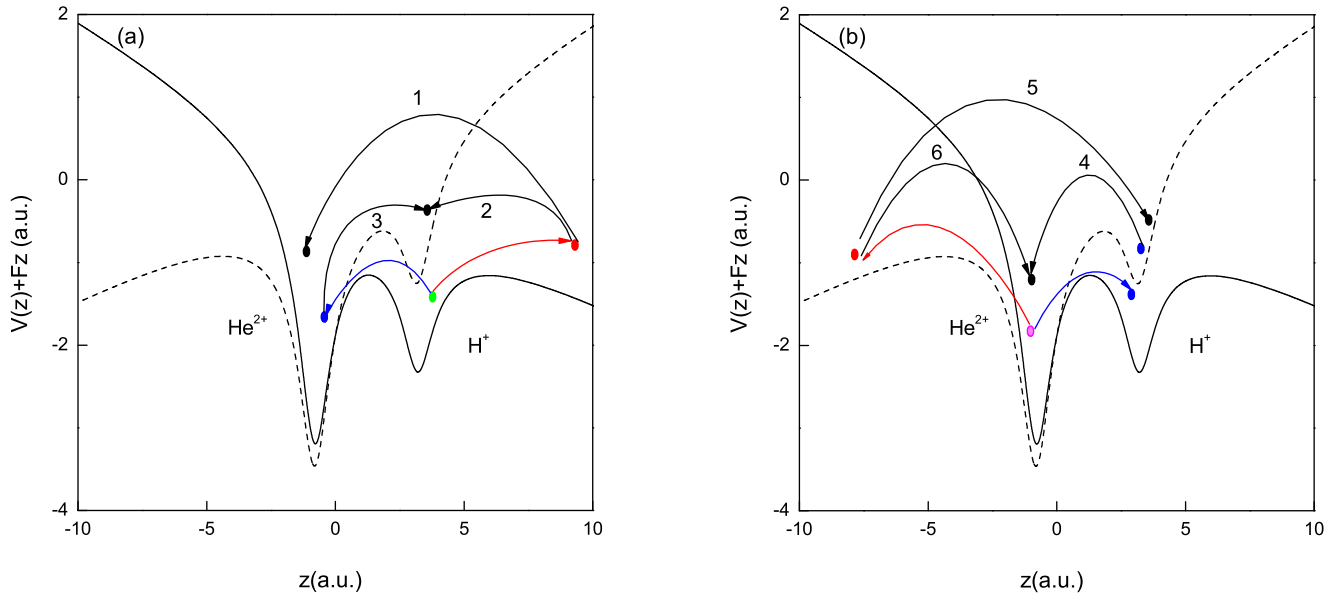


FIG. 1. (Color online) Schematic illustration of multichannel recombination in harmonic emission from $HeH^{2+}$. (a) and (b) are recombination channels originating from the excited $2p\sigma$ state (i.e., from the nucleus $H^+$) and from the ground $1s\sigma$ state (i.e., from the nucleus $He^{2+}$), respectively. The green (magenta) circles represent the electrons on the $2p\sigma$ state ($1s\sigma$ state), and red (black or blue) circles represent the ionized (recombined or transferred) electrons. The red (black or blue) lines illustrate the ionization (recombination or transfer) processes.

(channel 3: H $\rightarrow$ He $\rightarrow$ H) with the emission of harmonic photons. According to the three-step model [8–10], the harmonic energy depends closely on the acceleration process that the longer the acceleration the ionized electrons experience, the higher the harmonic energy is. Therefore the harmonic energies achieved via these three channels decrease in turn. Figure 1(b) describes the recombination channels originating from the ionized electrons on the $1s\sigma$ state (i.e., around the nucleus $He^{2+}$). When the laser field reaches the negative maximum (i.e., $F < 0$), some of the electrons located on the nucleus $He^{2+}$ will be pumped from the nucleus $He^{2+}$ to the nucleus $H^+$ due to resonance. After half an optical cycle, some excited electrons may transit back to the nucleus $He^{2+}$ (channel 4: He $\rightarrow$ H $\rightarrow$ He) with the emission of strong lower-order harmonic while others may be ionized directly from the nucleus $H^+$ and the related recombination channels have been introduced in the above. Besides being pumped to the nucleus $H^+$, some of the electrons located on the nucleus $He^{2+}$ can also be ionized; after the acceleration in the external field, the ionized electrons go back to recombine with the neighbor ion $H^+$ (channel 5: He $\rightarrow e \rightarrow$ H) or parent ion $He^{2+}$ (channel 6: He $\rightarrow e \rightarrow$ He) and emit the harmonic photons.

Based on the above analysis, all possible recombination channels from the $1s\sigma$ and $2p\sigma$ states have been obtained theoretically; we will try to distinguish the six recombination channels in harmonic emission from $HeH^{2+}$. Firstly, the trapezoidal laser pulse with lower laser intensity of $I = 8.0 \times 10^{13}$ W/cm$^2$ and the wavelength of 1200 nm shown in Fig. 2(a) is adopted. Figure 2(b) shows the initial electron-nuclear probability density distribution; $x$ and $y$ axes stand for the nuclear and electronic coordinates, respectively. Obviously, before interacting with the laser pulse, the electronic wave packets mainly locate in the region of $z > 0$. According to the description mentioned above, the electronic probability density distribution in the region of $z > 0$ describes the electronic wave packets in the $2p\sigma$ state moving around the nucleus $H^+$ while in the region of $z < 0$ it illustrates those on the $1s\sigma$ state moving around the nucleus $He^{2+}$. We use the formula

$$P(z,t) = \int_0^{R_{\max}} dR\,|\psi(R,z;t)|^2, \tag{12}$$

where $R_{\max}$ is the absorbing boundary. Electronic motion has been displayed in Fig. 2(c) by means of the time-dependent electronic probability density distribution. It can be seen that the electronic probability density almost distributes in part A at lower intensity. That is to say, when the system is exposed to the laser field with lower intensity, it mainly locates at the $2p\sigma$ state and the electrons move around the nucleus $H^+$. Due to the lower ionization potential of the $2p\sigma$ state, the electrons can still be ionized from the nucleus $H^+$ at lower laser intensity. In this case, three recombination channels shown in Fig. 1(a) may contribute to the HHG. In order to distinguish the recombination channels in harmonic emission, we have provided the corresponding time-frequency distribution in Fig. 2(d) based on Eq. (10). There are three obvious recombination channels that are displayed in the figure: Channel 1 with the highest harmonic energy results from the heteronuclear recombination H $\rightarrow e \rightarrow$ He; channel 2 is the homonuclear recombination, H $\rightarrow e \rightarrow$ H; and channel 3 with the lack of acceleration process owning the lowest harmonic energy is H $\rightarrow$ He $\rightarrow$ H. In short, the harmonic emission from $HeH^{2+}$ at lower intensity is mostly attributed to the three recombination channels from the $2p\sigma$ state. As is mentioned above, when the laser intensity is higher, the wave packets will be transferred between the $1s\sigma$ state and

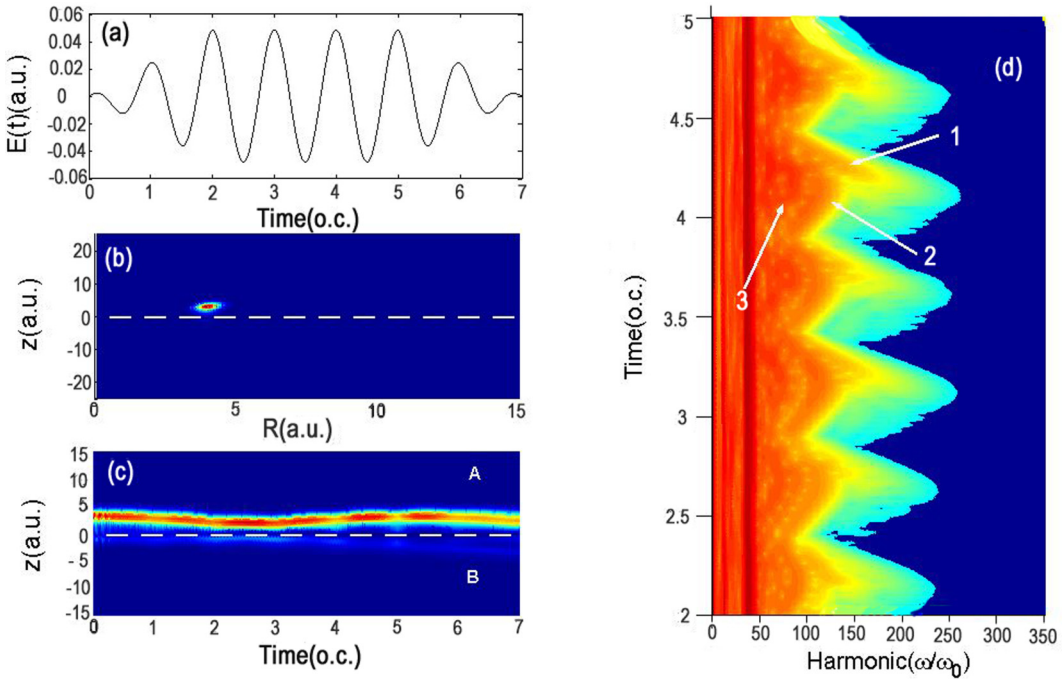


FIG. 2. (Color online) (a) Shape of laser field with the wavelength of 1200 nm and peak intensity of $I = 8.0 \times 10^{13}$ W/cm$^2$. The total pulse lasts for 7 o.c., and 1 o.c. = 4.005 fs equals the optical cycle of the wavelength with 1200 nm. (b) The initial electron-nuclear probability density distribution. (c) The electronic motion in the laser field displayed in (a), and (d) the corresponding time-frequency distribution from $t = 2$ o.c. to $t = 5$ o.c.

the $2p\sigma$ state. To distinguish the other three recombination channels in harmonic emission, the laser intensity is enhanced to a higher intensity of $I = 1.0 \times 10^{15}$ W/cm$^2$. Figure 3 offers the time evolution of the electron-nuclear probability density distributions from $t = 3.0$ o.c. to $t = 5.5$ o.c. at the first two rows, and the related time-frequency analysis at the third row. From the electron-nuclear probability density distributions, it is observed that comparable electrons move around the nucleus $He^{2+}$ around $t = n$ o.c. ($n$ is equal to 3, 4, and 5). Because the laser pulse reaches the positive peak intensity at $t = n$ o.c. as illustrated in Fig. 2(a) when the polarization direction is antiparallel to the permanent dipole of the $HeH^{2+}$, the electrons located in the potential of the nucleus $H^+$ can transit to the dressed-down potential of the nucleus $He^{2+}$ and be captured by the nucleus $He^{2+}$, which results in the large population around the nucleus $He^{2+}$. However, when the laser field changes its direction at $t = (n + 0.5)$ o.c., the potential of the nucleus $He^{2+}$ is dressed up while the potential of the nucleus $H^+$ is dressed down. Consequently, it is much more difficult for the electrons around the nucleus $H^+$ to be captured by the nucleus $He^{2+}$, and the corresponding electron-nuclear probability density is less than that around $t = n$ o.c. It is interesting that the electronic distribution around the two nuclei changes periodically at higher intensity which is dramatically different from that at lower intensity, and the related variation of recombination channels in HHG does attract our attention.

As displayed in the time-frequency distribution in Fig. 3, six recombination channels are extremely noticeable. Compared with the electronic probability density distribution at lower intensity shown in Fig. 2(c), the population of electrons around the nucleus $He^{2+}$ at higher intensity is large enough to exert significant influence on the recombination channels. The additional channels are probably ascribed to the electronic motion around the nucleus $He^{2+}$. Channel 4, with the lowest harmonic energy, appears periodically around $t = n$ o.c., for example, $t = 4.0$ o.c. It is closely related to the process of electron transfer from the nucleus $He^{2+}$ to the nucleus $H^+$. Around $t = 3.5$ o.c., the electrons located in the dressed-up potential of the nucleus $He^{2+}$ can be pumped to the dressed-down potential of the nucleus $H^+$; as the laser field changes its direction after half an optical cycle (i.e., around $t = 4.0$ o.c.), the potential of the nucleus $He^{2+}$ is dressed down and the potential of the nucleus $H^+$ is dressed up, and then the electrons may directly return to recombine with the nucleus $He^{2+}$. This induces the appearance of a strong $1s\sigma$-$2p\sigma$ resonance, namely, the recombination channel He $\rightarrow$ H $\rightarrow$ He introduced in Fig. 1(b), and it mainly contributes to the lower harmonic orders with strong intensity. For the other two recombination channels—based on the classical theory that the maximum harmonic energy of the individual channel is associated with the acceleration process in external field—channel 5 with later recombination time and higher harmonic energy corresponds to the heteronuclear recombination (He $\rightarrow e \rightarrow$ H) while channel 6 with earlier recombination time and lower harmonic energy is thought to be the homonuclear recombination (He $\rightarrow e \rightarrow$ He). Moreover, the quantum explanation based on the electron-nuclear probability density distribution verifies the distinguishing of recombination channels. The intensities of these two channels change periodically so that the intensities around $t = (n + 0.5)$ o.c. are stronger than those around $t = n$ o.c. For example, the intensity around $t = 3.5$ o.c. (related to the ionization time around $t_i = 3.0$ o.c.) is much more

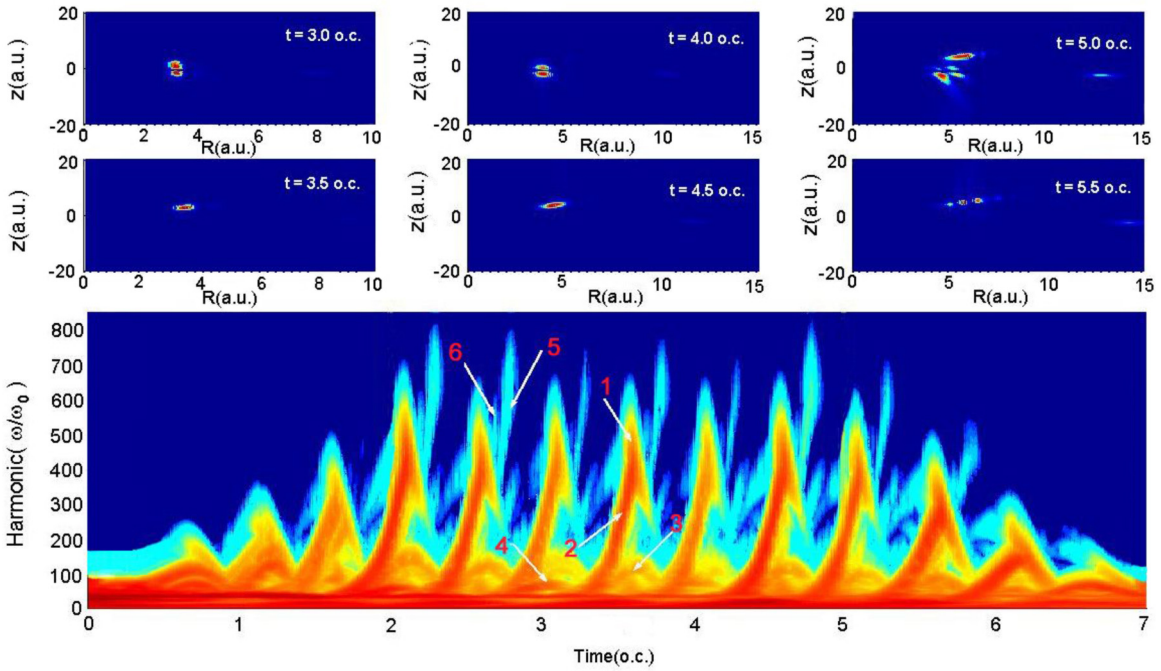


FIG. 3. (Color online) The first and second rows show the electron-nuclear probability density distributions at $t = n$ o.c. and $t = (n + 0.5)$ o.c. ($n = 3$, 4, and 5) for the higher laser intensity of $I = 1.0 \times 10^{15}$ W/cm$^2$, respectively. The third row is the corresponding time-frequency distribution with the identical laser parameters.

intensive than that around $t = 4.0$ o.c ($t_i = 3.5$ o.c.). As depicted in the electron-nuclear probability density distributions in Fig. 3, the intensity of the electronic probability density on the nucleus $He^{2+}$ around $t_i = 3.0$ o.c. is stronger than that around $t_i = 3.5$ o.c.; furthermore, the polarization of the laser field is antiparallel to the permanent dipole of the $HeH^{2+}$ at $t = 3.0$ o.c. when the potential well of the nucleus $He^{2+}$ is dressed down. Accordingly, the higher ionization probability from the nucleus $He^{2+}$ around $t_i = 3.0$ o.c. can be obtained, and it increases the relative contributions from these two channels around $t = 3.5$ o.c. What is unclear is whether the recombination with the neighbor ion ($H^+$) or with the parent ion ($He^{2+}$) leads to the formation of channel 5. Considering the higher intensities of channel 5 than channel 6 around $t = (n + 0.5)$ o.c., the probabilities of the electrons around nucleus $H^+$ are larger than those around nucleus $He^{2+}$ around $t = (n + 0.5)$ o.c., such as the electron-nuclear probability density distributions around $t = 3.5$ o.c. ($t = 4.5$ o.c. or $t = 5.5$ o.c.). As a consequence, the recombination with the nucleus $H^+$ (He $\rightarrow e \rightarrow$ H) corresponds to channel 5, while the recombination with the nucleus $He^{2+}$ corresponds to channel 6.

### B. Role of the recombination channels on harmonic emission

Based on the discussion about the multichannel recombination in harmonic emission mentioned above, it is found that the laser intensity prominently affects the recombination channels, and then these channels perhaps present different dynamic behaviors with the variation of laser intensity. So the contributions of different recombination channels to harmonic emissions are estimated by increasing the laser intensity in this part.

Due to the periodical harmonic emission, time-frequency distribution in one optical cycle (from 3.0 to 4.0 o.c.), shown in Fig. 4, is selected for the investigation. It can be seen that recombination channels contribute to different harmonic orders at different moments. For example, channel 4 (He $\rightarrow$ H $\rightarrow$ He) primarily rules the 60th harmonic around 3.0 o.c. Similarly, channel 3 (H $\rightarrow$ He $\rightarrow$ H) [channel 2 (H $\rightarrow e \rightarrow$ H) or channel 5 (He $\rightarrow$ e $\rightarrow$ H)] mainly dominates the 110th (200th or 600th) harmonic around 3.6 o.c. (3.5 o.c. or 3.8 o.c.), and channel 1 (H $\rightarrow e \rightarrow$ He) and channel 6 (He $\rightarrow e \rightarrow$ He) almost control the 400th harmonic around 3.5 and 3.65 o.c., respectively. Accordingly, the harmonic intensities at those selected emission times can be used to

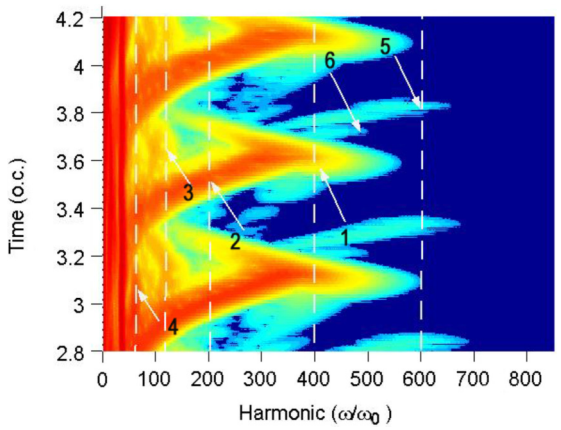


FIG. 4. (Color online) The time-frequency distribution for the laser intensity of $I = 7.0 \times 10^{14}$ W/cm$^2$ from $t = 2.8$ o.c. to $t = 4.2$ o.c.

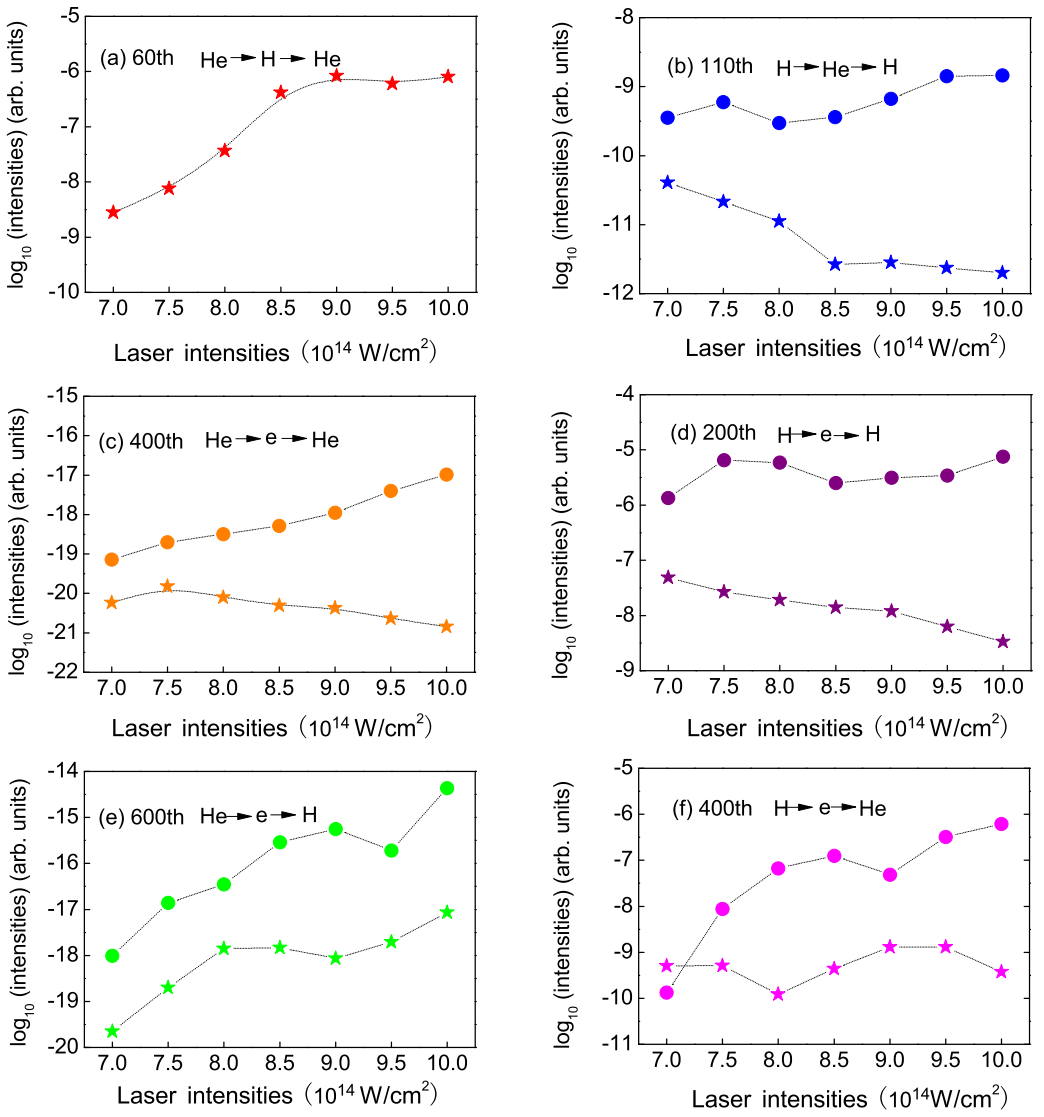


FIG. 5. (Color online) (a)–(f) display the variations of the intensities for the six channels by increasing the laser intensities from $7.0 \times 10^{14}$ to $1.0 \times 10^{15}$ W/cm$^2$ with the intensity spacing of $5.0 \times 10^{13}$ W/cm$^2$. The five-pointed star (circle) represents the first recombination (second recombination) in an optical cycle.

present the contributions of the corresponding recombination channels. Furthermore, it can be also observed from Fig. 4 that the effects of different channels on two recombinations in an optical cycle are not identical. Especially for channel 4, it barely affects the harmonic emission in the second recombination whereas it does in the first recombination. To gain deeper insight into the contributions of different channels to harmonic emission, Fig. 5 exhibits the related variations about the intensities of six recombination channels in the first recombination (five-pointed star) and the second recombination (circle) by increasing the laser intensity from $7.0 \times 10^{14}$ to $1.0 \times 10^{15}$ W/cm$^2$.

As depicted in Figs. 5(a) and 5(b), the He $\rightarrow$ H $\rightarrow$ He channel and the H $\rightarrow$ He $\rightarrow$ H channel mainly contributing to the lower-order harmonics relate to the process of electron transfer between the $1s\sigma$ and $2p\sigma$ states, namely, the electron transfer between the nucleus $He^{2+}$ and the nucleus $H^+$. The He $\rightarrow$ H $\rightarrow$ He channel appears mainly around $t = 3.0$ o.c., and the harmonic intensity is growing with the increase of the laser intensity. Furthermore, it is almost three magnitude orders stronger for the laser intensity of $I = 1.0 \times 10^{15}$ W/cm$^2$ than that for $I = 7.0 \times 10^{14}$ W/cm$^2$. The higher potential well of the nucleus $He^{2+}$ for stronger laser intensity [blue line in Fig. 6(b)] at $t = 2.5$ o.c. ($F < 0$) leads to a larger portion of electrons transferring from the nucleus $He^{2+}$ to the nucleus $H^+$. When the laser field changes its direction at $t = 3.0$ o.c., the much larger probability of electrons returning to the nucleus $He^{2+}$ probably results in the stronger power of the He $\rightarrow$ H $\rightarrow$ He channel. This process corresponds to the resonance between the $1s\sigma$ and $2p\sigma$ states. However, when the potential well of the nucleus $He^{2+}$ is dressed down and the potential well of the nucleus $H^+$ is dressed up at $t = 3.0$ o.c., there is little probability of the electrons around the nucleus $He^{2+}$ transferred to the nucleus $H^+$. As a result, it is almost invisible for the He $\rightarrow$ H $\rightarrow$ He channel in second recombination. With the similar mechanism, the H $\rightarrow$ He $\rightarrow$ H channel is

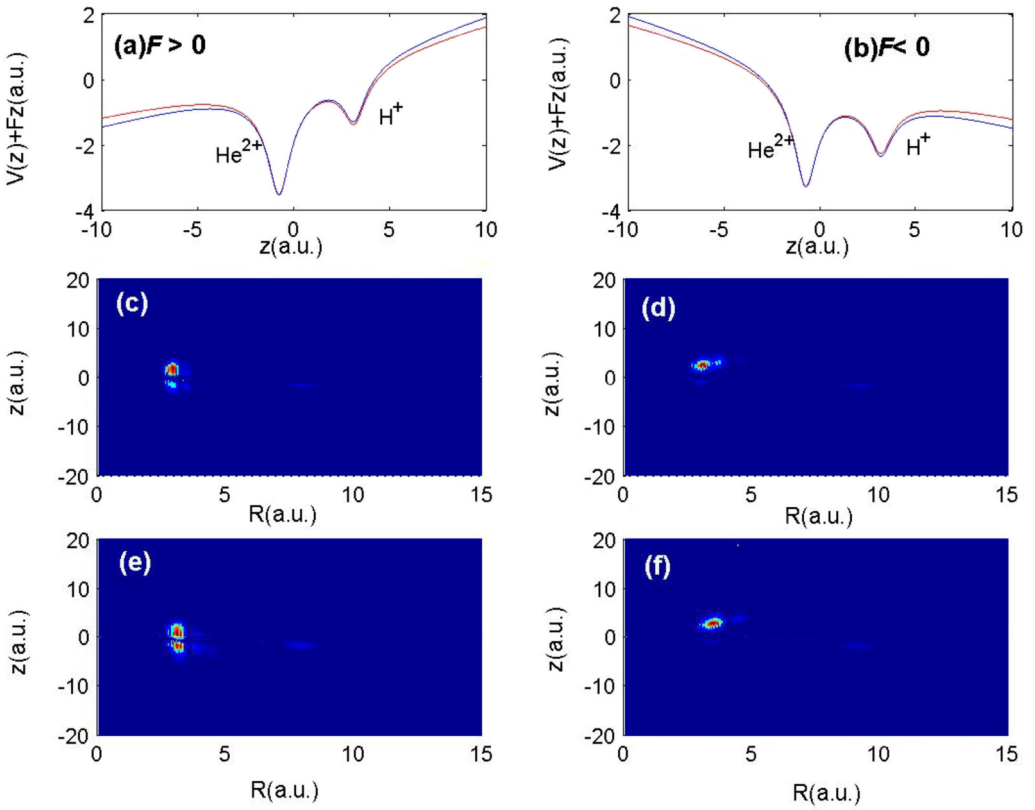


FIG. 6. (Color online) Combined Coulomb and static field potential for (a) $F > 0$ and (b) $F < 0$ for two laser intensities: $7.0 \times 10^{14}$ W/cm$^2$ (red line) and $1.0 \times 10^{15}$ W/cm$^2$ (blue line), respectively. (c) and (d) [(e) and (f)] are the electron-nuclear probability density distributions for $I = 7.0 \times 10^{14}$ W/cm$^2$ ($I = 1.0 \times 10^{15}$ W/cm$^2$) at $t = 3$ o.c. and $t = 3.8$ o.c., respectively.

sensitive to the variations of the laser intensities where the corresponding intensity mainly decreases (increases) with the growing of the laser intensity for the first recombination (the second recombination).

Differing from the He $\rightarrow$ H $\rightarrow$ He and the H $\rightarrow$ He $\rightarrow$ H channels, the other four recombination channels contributing to the plateau and cutoff regions of the harmonic spectrum relate to the ionization-acceleration-recombination process. Figures 5(c) and 5(e) display the variations of the intensities for the homonuclear recombination channel (He $\rightarrow e \rightarrow$ He) and the heteronuclear recombination channel (He $\rightarrow e \rightarrow$ H) originating from the $1s\sigma$ state. Obviously, the He $\rightarrow e \rightarrow$ He channel is sensitive to the laser intensity in the second recombination, and the corresponding recombination intensity is enhanced from $-19.1$ to $-16.9$. The recombination originates from the ejected electrons around $t_i = 3.0$ o.c. ($F > 0$) when the potential well of the nucleus $He^{2+}$ is dressed down lower for higher laser intensity (blue line) illustrated in Fig. 6(a). Moreover, the electronic probability density around the nucleus $He^{2+}$ for $I = 1.0 \times 10^{15}$ W/cm$^2$ [shown in Fig. 6(e)] is larger than that for $I = 7.0 \times 10^{14}$ W/cm$^2$ [shown in Fig. 6(c)]. These two factors result in the higher ionization probability from the nucleus $He^{2+}$ at higher laser intensity, and then more ionized electrons return and recombine with the parent ion $He^{2+}$; additionally, the intensity of the He $\rightarrow e \rightarrow$ He channel increases almost 2.2 magnitude orders for $I = 1.0 \times 10^{15}$ W/cm$^2$. Based on a similar mechanism, the intensity of the He $\rightarrow e \rightarrow$ H channel is much more sensitive to the variations of the laser intensities in the second recombination, and the recombination intensity increases from $-18.1$ to $-14.4$. With large numbers of the electrons ionized from the nucleus $He^{2+}$ around $t_i = 3.0$ o.c. ($F > 0$), more electrons will recombine with the nucleus $H^+$. It coincides well with the electron-nuclear probability density distribution in Figs. 6(d) and 6(f) showing that the electronic probability density around the nucleus $H^+$ around $t = 3.8$ o.c. for $I = 1.0 \times 10^{15}$ W/cm$^2$ is larger than that for $I = 7.0 \times 10^{14}$ W/cm$^2$. Moreover, by comparing the intensities of the He $\rightarrow e \rightarrow$ H channel with that of the He $\rightarrow e \rightarrow$ He channel for two recombinations in one optical cycle, we can find that the intensity of the former is much stronger than that of the latter, and the difference between the intensity of these two channels is enhanced with the increase of the laser intensity. It may be summarized that the ionized electrons from the nucleus $He^{2+}$ tend to recombine with the nucleus $H^+$ in the harmonic emission. In other words, the He $\rightarrow e \rightarrow$ H channel dominates when the initial ionization processes are based on the $1s\sigma$ state. For the homonuclear recombination channel (H $\rightarrow e \rightarrow$ H) and the heteronuclear recombination channel (H $\rightarrow e \rightarrow$ He) originating from the $2p\sigma$ state illustrated in Figs. 5(d) and 5(f), the H $\rightarrow e \rightarrow$ H channel is sensitive to the laser intensity in the first recombination, and it decreases faster than the He $\rightarrow e \rightarrow$ H channel. This is because whether the electrons are ionized from the nucleus $He^{2+}$ or from the nucleus $H^+$ is dramatically affected by the laser dressed potential, and the recombination channels from

the $2p\sigma$ state compete with those from the $1s\sigma$ state. It is worth noting that the intensity of the H $\rightarrow e \rightarrow$ H channel in the second recombination is several magnitude orders stronger than that in the first recombination; moreover, it tends to be much stronger around $t = 3.5$ o.c. with increasing the laser intensity. While the H $\rightarrow e \rightarrow$ He channel is sensitive to the laser intensity in the second recombination demonstrated in Fig. 5(f), the recombination intensity is enhanced greatly from $-9.9$ to $-6.2$. Despite the 3.7 magnitude orders enhancement of the intensity for the H $\rightarrow e \rightarrow$ He channel, the H $\rightarrow e \rightarrow$ H channel with the strongest intensity dominates among the recombination channels from the $2p\sigma$ state.

## IV. CONCLUSIONS

In summary, the investigation of the multichannel recombination in harmonic emission from the asymmetric molecular ion has been performed by numerically solving the time-dependent Schrödinger equation based on the non-Born-Oppenheimer approximation. The results show that with the transition of the wave packets between the ground and first excited states, the electrons can be ionized either from the ground state (i.e., from the nucleus $He^{2+}$) or from the first excited state (i.e., from the nucleus $H^+$), and then multichannel recombination may contribute to the harmonic emission. By changing the laser intensity, the six recombination channels have been found and distinguished. Moreover, these channels from different electronic states have different effects on the harmonic emission. For the initial ionization from the first excited state, the H $\rightarrow e \rightarrow$ H channel dominates while from the ground state the He $\rightarrow e \rightarrow$ H channel does.

## ACKNOWLEDGMENTS

The authors sincerely thank Professor Keli Han and Dr. Ruifeng Lu for providing us the LZH-DICP code. This work is supported by the Special Funds of the National Natural Science Foundation of China (Grant No. 11047191), Key Project of Chinese Ministry of Education (Grant No. 211025), Research Fund for the Doctoral Program of Higher Education of China (Grant No. 20111404120004), the Natural Science Foundation for Young Scientists of Shanxi Province, China (Grant No. 2009021005), and Innovation Project for Postgraduates of Shanxi Province, China (Grant No. 20133100).

[1] T. Brabec and F. Krausz, Rev. Mod. Phys. **72**, 545 (2000).
[2] F. Krausz and M. Ivanov, Rev. Mod. Phys. **81**, 163 (2009).
[3] Z. Chang and P. Corkum, J. Opt. Soc. Am. B **27**, B9 (2010).
[4] P. B. Corkum and F. Krausz, Nat. Phys. **3**, 381 (2007).
[5] J. Itatani, J. Levesque, D. Zeidler, Hiromichi Niikura, H. Pepin, J. C. Kieffer, P. B. Corkum, and D. M. Villeneuve, Nature (London) **432**, 867 (2004).
[6] H. Niikura, D. M. Villeneuve, and P. B. Corkum, Phys. Rev. Lett. **94**, 083003 (2005).
[7] M. V. Frolov, N. L. Manakov, T. S. Sarantseva, M. Yu. Emelin, M. Yu. Ryabikin, and A. F. Starace, Phys. Rev. Lett. **102**, 243901 (2009).
[8] P. B. Corkum, Phys. Rev. Lett. **71**, 1994 (1993).
[9] H. N. Du and X. Y. Miao, Spectrosc. Lett. **45**, 609 (2012).
[10] H. N. Du and X. Y. Miao, Spectrosc. Lett. **45**, 556 (2012).
[11] L. Q. Feng and T. S. Chu, Commun. Comput. Chem. **1**, 52 (2013).
[12] Y. J. Chen, J. Liu, and B. Hu, Phys. Rev. A **79**, 033405 (2009).
[13] Y. C. Han and L. B. Madsen, J. Phys. B **43**, 225601 (2010).
[14] J. Bao, W. B. Chen, Z. X. Zhao, and J. M. Yuan, J. Phys. B **44**, 195601 (2011).
[15] Y. C. Han and L. B. Madsen, Phys. Rev. A **87**, 043404 (2013).
[16] I. Ben-Itzhak, I. Gertner, O. Heber, and B. Rosner, Phys. Rev. Lett. **71**, 1347 (1993).
[17] I. Ben-Itzhak, J. P. Bouhnik, B. D. Esry, I. Gertner, O. Heber, and B. Rosner, Phys. Rev. A **54**, 474 (1996).
[18] I. Ben-Itzhak, Z. Chen, B. D. Esry, I. Gertner, O. Heber, C. D. Lin, and B. Rosner, Phys. Rev. A **49**, 1774 (1994).
[19] X. B. Bian and A. D. Bandrauk, Phys. Rev. Lett. **105**, 093903 (2010).
[20] X. B. Bian and A. D. Bandrauk, Phys. Rev. A **83**, 023414 (2011).
[21] X. B. Bian and A. D. Bandrauk, Phys. Rev. A **83**, 041403(R) (2011).
[22] X. B. Bian and A. D. Bandrauk, Phys. Rev. A **86**, 053417 (2012).
[23] Y. J. Chen and B. Zhang, Phys. Rev. A **86**, 023415 (2012).
[24] R. F. Lu, C. Yu, Y. H. Wang, Q. Shi, and Y. D. Zhang, Phys. Lett. A **378**, 90 (2014).
[25] C. D. Liu, Z. N. Zeng, P. F. Wei, P. Liu, R. X. Li, and Z. Z. Xu, Phys. Rev. A **81**, 033426 (2010).
[26] T. Kreibich, M. Lein, V. Engel, and E. K. U. Gross, Phys. Rev. Lett. **87**, 103901 (2001).
[27] X.-Y. Miao and H.-N. Du, Phys. Rev. A **87**, 053403 (2013).
[28] K. L. Liu, W. Y. Hong, and P. X. Lu, Opt. Express **19**, 20279 (2011).
[29] V. Roudnev, B. D. Esry, and I. Ben-Itzhak, Phys. Rev. Lett. **93**, 163601 (2004).
[30] R. F. Lu, C. Y. Xiao, K. M. Deng, and H. P. Wu, Chem. Phys. **382**, 88 (2011).
[31] H. X. He, R. F. Lu, P. Y. Zhang, K. L. Han, and G. Z. He, J. Phys. B: At. Mol. Opt. Phys. **45**, 085103 (2012).
[32] R. F. Lu, P. Y. Zhang, and K. L. Han, Phys. Rev. E **77**, 066701 (2008).
[33] P. Y. Zhang, R. F. Lu, A. J. Zhang, T. S. Chu, and K. L. Han, J. Chem. Phys. **128**, 091103 (2008).
[34] H. X. He, R. F. Lu, P. Y. Zhang, K. L. Han, and G. Z. He, J. Chem. Phys. **136**, 024311 (2012).
[35] H. X. He, R. F. Lu, P. Y. Zhang, Y. H. Guo, K. L. Han, and G. Z. He, Phys. Rev. A **84**, 033418 (2011).
[36] K. Burnett, V. C. Reed, J. Cooper, and P. L. Knight, Phys. Rev. A **45**, 3347 (1992).
[37] X. M. Tong and Shih-I Chu, Phys. Rev. A **61**, 021802(R) (2000).
[38] X. Chu and Shih-I Chu, Phys. Rev. A **64**, 021403(R) (2001).